Gomis, O.; Manjón, F.; Rodríguez-Hernández, P.; Muñoz, A. (2019). Elastic and thermodynamic properties of alpha-Bi2O3 at high pressures: Study of mechanical and dynamical stability. Journal of Physics and Chemistry of Solids. 124:111-120. https://doi.org/10.1016/j.jpcs.2018.09.002

Elastic and thermodynamic properties of α-Bi_2O_3 at high pressures: study of mechanical and dynamical stability

O. Gomis,[a,*] F. J. Manjón,[b] P. Rodríguez-Hernández,[c] A. Muñoz[c]

[a]*Centro de Tecnologías Físicas: Acústica, Materiales y Astrofísica, MALTA Consolider Team, Universitat Politècnica de València, 46022 València, Spain*

[b]*Instituto de Diseño para la Fabricación y Producción Automatizada, MALTA Consolider Team, Universitat Politècnica de València, 46022 València, Spain*

[c]*Departamento de Física, Instituto de Materiales y Nanotecnología, MALTA Consolider Team, Universidad de La Laguna, 38200 La Laguna, Tenerife, Spain*

* Corresponding author. Tel.: +34 96 652 8426; fax: +34 96 652 8485.

E-mail address: osgohi@fis.upv.es (Oscar Gomis)

Dr. Oscar Gomis

Departamento de Física Aplicada

Escuela Politécnica Superior de Alcoy

Universitat Politècnica de València

Placeta Ferrandiz Carbonell 2

03802 Alcoy (Alicante)

Spain

Abstract

The elastic and thermodynamic properties of the monoclinic polymorph of bismuth oxide (α-Bi_2O_3); aka mineral bismite, have been theoretically investigated both at room pressure and under hydrostatic compression by means of first principles calculations based on density functional theory. In this work, the elastic stiffness coefficients, elastic moduli, Poisson's ratio, *B/G* ratio, elastic anisotropy indexes (A_B, A_G, A_1, A_2, A_3, A_U) and directional dependence of Young modulus and linear compressibility have been obtained. Vickers hardness, and sound wave velocities have been calculated. Our simulations show that bismite has a high elastic anisotropy. α-Bi_2O_3 is a ductile material whose elastic anisotropy increases under compression and presents a stronger ability to resist volume compression than shear deformation at all pressures. Besides, it has a very small minimum thermal conductivity, which is well suited for thermoelectric applications. Finally, the mechanical and dynamical stability of bismite at high pressure has been studied and it has been found that α-Bi_2O_3 becomes mechanically unstable at pressures beyond 19.3 GPa and dynamically unstable above 11.5 GPa. These instabilities could be responsible for the amorphization of bismite observed experimentally between 15 and 20 GPa.

Keywords:

oxides

ab initio calculations

high pressure

elastic properties

thermodynamic properties

1. Introduction

Bismuth trioxide has been extensively studied due to its high polymorphism and technological importance **[1]**. The stable phase of Bi_2O_3 at room conditions is the α phase, which occurs in nature as mineral bismite. α-Bi_2O_3 crystallizes in a monoclinic crystalline structure (space group: $P2_1/c$ No. 14, Z=4) and this phase presents the lowest symmetry of all the known polymorphs of bismuth trioxide **[1, 2]**. The structure of α-Bi_2O_3 can be described as layers of bismuth atoms parallel to the (100) plane of the monoclinic cell, separated by layers of oxygen atoms (see **Fig. 1**) **[1]**. Noteworthy, recent studies on α-Bi_2O_3 have focused on its use as a photocatalyst, a gas sensor and a supercapacitor **[3-7]**.

The structural, vibrational, optical, electric and magnetic properties of α-Bi_2O_3 have been studied under different conditions of temperature or pressure **[1, 8-23]**. These studies report that this material has unusual magnetic and electrical properties such as the existence of internal magnetic fields and a longitudinal magnetoelectric effect **[9, 10]**. In addition, shock compression experiments have demonstrated that bismite can be used as thermite mixtures for high pressure (HP) applications **[8]**. In this context, powder X-ray diffraction and Raman scattering experiments have shown that α-Bi_2O_3 undergoes an amorphization at HP between 15 and 20 GPa depending on the hydrostatic conditions **[16, 22, 23]**.

Despite the technological applicability of α-Bi_2O_3, its elastic properties are barely known and, to the best of our knowledge, only its axial compressibilities, bulk modulus at zero pressure, and sound velocity are recently known **[8, 16]**. The present work reports a theoretical study of the elastic and thermodynamic properties of bismite both at room pressure (0.0001 GPa) and at HP up to ~20 GPa. This study has allowed us to discuss the mechanical stability of this sesquioxide at HP. Besides, we report lattice

dynamics *ab initio* calculations at different pressures. In particular, the knowledge of the phonon dispersion curves (PDCs) at different pressures has allowed us to study the dynamical stability of bismite at HP. We will show that the monoclinic structure of Bi_2O_3 becomes dynamically unstable prior to become mechanically unstable. These instabilities likely cause the amorphization experimentally observed in α-Bi_2O_3 between 15 and 20 GPa.

2. Calculation methods

Ab initio simulations of α-Bi_2O_3 under compression were carried out with the density functional theory (DFT) **[24]** employing the plane-wave pseudopotential method implemented in the VASP code (Vienna *Ab initio* Simulation Package) **[25]**. The use of the projector-augmented wave scheme (PAW) **[26]** has allowed us to describe the full nodal character of the all-electron charge density in the core region taking into account 15 valence electrons ($5d^{10}6s^24p^3$) for bismuth and 6 valence electrons ($2s^22p^4$) for oxygen. The exchange-correlation energy was computed within the generalized gradient approximation (GGA) using the Perdew-Burke-Ernzenhof functional for solids (PBEsol) **[27].** A 6 x 4 x 4 Monkhorst–Pack grid of special k-points was used for integrations over the Brillouin zone (BZ). In order to obtain accurate results for a precise description of the electronic properties, the basis set of plane waves was developed up to an energy cutoff of 520 eV. In this way, a high convergence in total energy (better than 1 meV per formula unit) was obtained. Our calculations do not take into account the spin-orbit interaction because those calculations are computationally very demanding and it has been previously shown that spin-orbit interaction is small in α-Bi_2O_3 **[23]**.

DFT calculations are a well-tested method that describes properly the properties of semiconductors under compression **[28]**. For that purpose, the structure of bismite was fully relaxed to its optimized configuration at several chosen volumes (or equivalently pressures) through the calculation of forces on atoms and stress tensors. In this way, the structural parameters were obtained, as well as a set of related energies, volumes, and pressures. For each optimized structure, Hellmann-Feynman forces on atoms were smaller than 0.006 eV/Å, and the deviation of the stress tensor from the diagonal hydrostatic form was lower than 0.1 GPa. The simulations also provided the formation energy and cohesive energy of α-Bi_2O_3, -6.531 eV and 2.947 eV, respectively; in good agreement with experimental results **[29]**.

The elastic constants were evaluated by computing the macroscopic stress for a small strain applying the stress theorem **[30, 31]** as implemented in the VASP code. Taking into account their symmetry, the ground state and the optimized structures are strained in different directions **[32]**. A Taylor expansion of the total energy with respect to the applied strain is used to evaluate with high precision the small total-energy differences between different strained states **[33]**. During the simulations some tests were performed using small strains in order to ensure the harmonic approximation from the strain-stress relationship. We have also studied the mechanical properties of α-Bi_2O_3 using the elastic moduli obtained from the calculated elastic constants.

Finally, the dynamical stability of α-Bi_2O_3 was studied with *ab initio* DFT-based lattice-dynamics simulations at the zone centre (Γ point) and along high symmetry directions of the BZ by using the PHONON code **[34]**. To calculate the dynamical matrix using the harmonic approximation with the direct force constant approach, highly converged results on forces are required **[34, 35]**. The PDCs were obtained with

a supercell of size 2 x 2 x 4 (320 atoms) that gave a good description of the phonon branches.

3. Results and discussion

3.1. Elastic properties and mechanical stability of bismite

α-Bi_2O_3 has 13 independent second-order elastic constants (C_{ij}) which, in the Voigt notation, are: C_{11}, C_{12}, C_{13}, C_{15}, C_{22}, C_{23}, C_{25}, C_{33}, C_{35}, C_{44}, C_{46}, C_{55} and C_{66} **[36]**. When the crystal is loaded under external hydrostatic compression, the elastic stiffness coefficients, B_{ij}, must be employed instead of C_{ij} elastic constants. The B_{ij} coefficients for a monoclinic crystal, in the Voigt notation, under an external hydrostatic pressure, P, are: $B_{11} = C_{11} - P$, $B_{12} = C_{12} + P$, $B_{13} = C_{13} + P$, $B_{15} = C_{15}$, $B_{22} = C_{22} - P$, $B_{23} = C_{23} + P$, $B_{25} = C_{25}$, $B_{33} = C_{33} - P$, $B_{35} = C_{35}$, $B_{44} = C_{44} - P$, $B_{46} = C_{46}$, $B_{55} = C_{55} - P$ and $B_{66} = C_{66} - P$ **[37]**. Note that the values of B_{ij} and C_{ij} are equal when P = 0 GPa (value close to room pressure).

a) At room pressure

Table 1 lists the calculated C_{ij} elastic constants for α-Bi_2O_3 at 0 GPa. Elastic constants are referred to an orthonormal coordinate system (x, y, z) **[36]**. These orthonormal axes, following the IRE (Institute of Radio Engineers) convention, are related to the monoclinic crystal lattice vectors (***a***, ***b***, ***c***) in the following way: y-axis is parallel to b-axis, z-axis is parallel to c-axis, and x-axis is perpendicular to (yz) plane. C_{11}, C_{22} and C_{33} elastic constants indicate the resistance of the material to be elongated or compressed along x, y and z directions, respectively. For α-Bi_2O_3, $C_{33} > C_{11} > C_{22}$ indicates that unidirectional compressibility increases in the following sequence of directions: [001] < [100] < [010]. On the other hand, elastic constants C_{44}, C_{55} and C_{66} are related to the resistance to shear deformation. In our particular case, $C_{66} > C_{55} > C_{44}$

153 denotes that the [010](001) shear is easier than the [001](100) shear which is easier than
154 the [100](010) shear. C_{11}, C_{22} and C_{33} are greater than C_{44}, C_{55} and C_{66} in bismite. This
155 indicates that this material has a greater resistance to unidirectional compression than to
156 shear deformation. Finally, elastic constants with mixed compression/shear coupling
157 (C_{15}, C_{25} and C_{35}) along with elastic constant C_{46} related to shear deformation have the
158 smallest values in bismite.

159 The calculated elastic constants for α-Bi_2O_3 can be compared to those
160 experimentally obtained for glass Bi_2O_3 using the pulse echo overlap technique **[38]**.
161 The value of C_{11} in the glass (C_{11} = 86.5 GPa) is 26% smaller than the theoretical
162 average (C_{11} + C_{22} + C_{33})/3 in the crystal. The value of C_{44} in the glass (C_{44} = 26.5 GPa)
163 is 30% smaller than the theoretical average (C_{44} + C_{55} + C_{66})/3 in the crystal. These
164 results clearly suggest that the crystalline phase is stiffer than the glass, as observed in a
165 number of compounds **[39]**, and give confidence to our calculated results to continue
166 exploring the mechanical properties of bismite from a theoretical ground.

167 The knowledge of the elastic constants at 0 GPa allows us to study the
168 mechanical stability of the monoclinic structure. In this context, the mechanical stability
169 of a crystal at zero pressure requires that the whole set of elastic constants, C_{ij}, satisfies
170 the Born stability criteria **[40]**. These stability criteria for monoclinic crystals with 13
171 independent elastic constants, taking into account that C_{ij} matrix must be positive-
172 definite, are given by the following conditions:

173 $$m_1 = C_{11} > 0 \quad (1)$$

174 $$m_2 = C_{11}C_{22} - C_{12}^2 > 0 \quad (2)$$

175 $$m_3 = (C_{22}C_{33} - C_{23}^2)C_{11} - C_{33}C_{12}^2 + 2C_{23}C_{12}C_{13} - C_{22}C_{13}^2 > 0 \quad (3)$$

176 $$m_4 = C_{44} > 0 \quad (4)$$

$$
\begin{aligned}
m_5 = {} & C_{12}^2 C_{35}^2 - C_{33} C_{55} C_{12}^2 + 2C_{55} C_{12} C_{13} C_{23} - 2C_{12} C_{13} C_{25} C_{35} \\
& - 2C_{12} C_{15} C_{23} C_{35} + 2C_{33} C_{12} C_{15} C_{25} + C_{13}^2 C_{25}^2 - C_{22} C_{55} C_{13}^2 \\
& - 2C_{13} C_{15} C_{23} C_{25} + 2C_{22} C_{13} C_{15} C_{35} + C_{15}^2 C_{23}^2 - C_{22} C_{33} C_{15}^2 \\
& - C_{11} C_{55} C_{23}^2 + 2C_{11} C_{23} C_{25} C_{35} - C_{11} C_{33} C_{25}^2 - C_{11} C_{22} C_{35}^2 \\
& + C_{11} C_{22} C_{33} C_{55} > 0
\end{aligned} \tag{5}
$$

$$
m_6 = C_{44} C_{66} - C_{46}^2 > 0 \tag{6}
$$

Values of m_i (i = 1-6) at 0 GPa are given in **Table 2**. As it can be observed, all the stability criteria are satisfied at 0 GPa; thus, the monoclinic structure of bismite is mechanically stable at room pressure. This result is in good agreement with the fact that mineral bismite is found at room conditions.

The elastic moduli can be obtained from the elastic stiffness coefficients B_{ij}. In particular, the bulk modulus, B, and shear modulus, G, have been calculated with the expressions **[41]**:

$$
B_V = \frac{B_{11} + B_{22} + B_{33} + 2(B_{12} + B_{23} + B_{13})}{9} \tag{7}
$$

$$
\frac{1}{B_R} = S_{11} + S_{22} + S_{33} + 2(S_{12} + S_{23} + S_{13}) \tag{8}
$$

$$
B_H = \frac{B_V + B_R}{2} \tag{9}
$$

$$
G_V = \frac{B_{11} + B_{22} + B_{33} - (B_{12} + B_{23} + B_{13}) + 3(B_{44} + B_{55} + B_{66})}{15} \tag{10}
$$

$$
\frac{1}{G_R} = \frac{4(S_{11} + S_{22} + S_{33}) - 4(S_{12} + S_{23} + S_{13}) + 3(S_{44} + S_{55} + S_{66})}{15} \tag{11}
$$

$$
G_H = \frac{G_V + G_R}{2} \tag{12}
$$

The elastic moduli are derived in the Voigt **[42]**, Reuss **[43],** and Hill **[44]** approximations labeled with subscripts V, R, and H, respectively; in **Eqs. 7-12**.

196 The Young modulus, E, has been obtained from the bulk and shear moduli with
197 the expression **[45]**:

198 $$E_X = \frac{9B_X G_X}{G_X + 3B_X} \quad (13)$$

199

200 The subscript X in **Eq. 13** refers to the symbols V, R, and H.

201 Elastic moduli in α-Bi_2O_3 at 0 GPa are tabulated in **Table 1**. It must be stressed
202 that the Hill bulk modulus, B_H = 68.3 GPa is in rather good agreement with the
203 theoretical value (B_0 = 72.8 GPa) obtained from our structural data calculated with
204 VASP. This agreement (there is only a 6% difference) suggests the consistency of our
205 calculations. On the other hand, our Hill bulk modulus is 20% smaller than the
206 experimental value of B_0 = 85.4 GPa previously reported **[16]**. It must be stressed that
207 the last two values for B_0 were obtained from a 3rd order Birch-Murnaghan equation of
208 state **[16]**. Besides, our calculated value for B_H is 36% smaller than the bulk modulus
209 obtained from shock compression experiments (B_0 = 106 GPa) **[8]**. In this context, it
210 should be commented that the small value of the first derivative of the bulk modulus,
211 B_0'= 1.28 found in the shock compression work results in a greater value for B_0 due to
212 the strong correlation between B_0 and B_0' **[46]**. The fact that the bulk modulus is greater
213 than the shear modulus indicates that α-Bi_2O_3 presents a stronger ability to resist
214 volume compression than shear deformation at 0 GPa.

215 The Poisson's ratio, v, is connected with the way structural elements are packed
216 and provides information about the characteristics of the bonding forces and chemical
217 bonding **[47]**. The v ratio has been calculated with the expression **[45]**:

218 $$v_X = \frac{1}{2}\left(\frac{3B_X - 2G_X}{3B_X + G_X}\right) \quad (14)$$

219

The subscript *X* in **Eq. 14** refers to the symbols *V*, *R*, and *H*. The Poisson's ratio in α-Bi_2O_3, with the Hill approximation, is $v = 0.29$ at 0 GPa (see **Table 1**). Since $v > 0.25$ the interatomic bonding forces are predominantly central and the ionic bonding prevails against covalent bonding in bismite at room pressure **[48, 49].**

The *B/G* ratio was proposed by Pugh as a relationship which relates empirically the plastic properties of a material with its elastic moduli **[50]**. This relationship quantifies the ratio between the resistance to fracture and the resistance to plastic deformation. A value of the *B/G* ratio higher (lower) than 1.75 is associated with a ductile (brittle) material. In our calculations, we have found a value of $B/G = 2.04$ for α-Bi_2O_3 at 0 GPa (see **Table 1**) which indicates that bismite is ductile at room pressure.

It is well known that microcracks may be induced in materials due to elastic anisotropy **[51].** We have evaluated this anisotropy using different anisotropy indexes. Firstly, we have calculated the percentage of anisotropy in both compressibility and shear moduli with expressions $A_B = (B_V - B_R)/ (B_V + B_R)$ and $A_G = (G_V - G_R)/ (G_V + G_R)$, respectively **[52]**. A value of 0% indicates no anisotropy, while a value of 100% is associated with the largest anisotropy. In α-Bi_2O_3, $A_B = 4.35\%$ and $A_G = 7.73\%$ at 0 GPa (see **Table 1**). These results indicate a larger anisotropy in shear than in compression in bismite at room pressure. Secondly, we have calculated the shear anisotropic factors that provide a measure of the degree of anisotropy in the bonding between atoms in different planes **[47]**. The formulas that define the shear anisotropy factors are the following:

$$A_1 = \frac{4B_{44}}{B_{11} + B_{33} - 2B_{13}} \tag{15}$$

$$A_2 = \frac{4B_{55}}{B_{22} + B_{33} - 2B_{23}} \tag{16}$$

$$A_3 = \frac{4B_{66}}{B_{11} + B_{22} - 2B_{12}} \tag{17}$$

where A_1 is the factor for the {100} shear planes between the ⟨011⟩ and ⟨010⟩ directions, A_2 is for the {010} shear planes between the ⟨101⟩ and ⟨001⟩ directions, and A_3 is for the {001} shear planes between the ⟨110⟩ and ⟨010⟩ directions **[47]**. For an isotropic crystal the shear anisotropy factors must be one. A value of A_1, A_2 or A_3 smaller or greater than one is a measure of the elastic anisotropy of the crystal. In α-Bi_2O_3, $A_1 = 0.80$, $A_2 = 0.84$ and $A_3 = 2.32$ at 0 GPa (see **Table 1**). These results indicate that bismite exhibits a larger anisotropy in A_3 and shows more distinct performance in {001} planes than in {100} and {010} planes. Thirdly, we have also calculated the anisotropy of the material by using the universal elastic anisotropy index A_U defined by: $A_U=5(G_V/G_R)+(B_V/B_R)-6$ **[53]**. For a locally isotropic crystal, A_U must be zero, so the deviation of A_U from zero is a measure of the degree of elastic anisotropy for the crystalline structure. We have found that α-Bi_2O_3 is elastically anisotropic because it has an A_U value above zero at 0 GPa (see **Table 1**).

The anisotropy in the monoclinic cell of bismite can also be estimated by the axial compressibilities κ_a, κ_b and κ_c. These compressibilities have been obtained by using the expressions **[36]:**

$$\kappa_a = S_{11} + S_{12} + S_{13} \tag{18}$$

$$\kappa_b = S_{12} + S_{22} + S_{23} \tag{19}$$

$$\kappa_c = S_{13} + S_{23} + S_{33} \tag{20}$$

where S_{ij} are the components of the elastic compliances tensor. **Table 3** includes the values for κ_a, κ_b and κ_c, obtained at 0 GPa using **Eqs. 18, 19** and **20**. It is found that $\kappa_b > \kappa_c > \kappa_a$; i.e., the *b*-axis is the most compressible one and the *a*-axis the less compressible one. Our theoretical results (see **Table 3**) are in good agreement with those given in

Ref. 16 obtained from equation of state fits. Therefore, this result again gives us confidence about the correctness of our simulations. The elastic anisotropy of bismite given by the different anisotropy indexes is in agreement with the anisotropy observed in the axial compressibilities, since $\kappa_c/\kappa_a > 1$ and $\kappa_b/\kappa_c > 1$.

To conclude with the study of the anisotropy, we have obtained the directional dependence of both the Young modulus, E, and the linear compressibility, κ, for bismite at 0 GPa using the ELATE program **[54]**. The results are shown in **Fig. 2** with a 3D parametric surface. For an absolutely isotropic medium this surface must be a sphere. It is clearly evidenced that α-Bi_2O_3 is highly anisotropic. The direction of minimum E, in Cartesian coordinates (x, y, z), is (0, 1, 0) [see **Table 4**]. This indicates that the direction with the smallest stiffness is along the b-axis. The stiffest direction is (0.30, 0, 0.95). This direction is in the (010) plane at an angle of 17.5º to the z-axis. The directions for maximum and minimum values of E (E_{max} and E_{min}) are correlated with the fact that $C_{33} > C_{11} > C_{22}$. The high anisotropy is also evidenced quantitatively by the ratio $E_{max} / E_{min} = 2.4$. On the other hand, the linear compressibility takes maximum and minimum values of $\kappa_{max} = 8.8$ TPa^{-1} and $\kappa_{min} = 1.7$ TPa^{-1} (see **Table 4**). The anisotropy ratio in linear compressibility is also quite high, $\kappa_{max} /\kappa_{min} = 5.1$. The direction of maximum compressibility is (0, 1, 0), that is, the b-axis. We note that κ_{max} has the same value as the axial compressibility $\kappa_b = 8.79 \cdot 10^{-3}$ GPa^{-1} (see **Table 3**). The direction of minimum compressibility is (0.89, 0, 0.45). This direction is in the (010) plane at an angle of 27.0º to the x-axis and 49.3º to the a-axis.

Another common mechanical magnitude to characterize materials is hardness. It is known that hardness is a complex variable which involves elasticity and plasticity in a material. It has been recently proposed that the Vickers hardness, H_v, can be obtained with the expression of Tian *et al*. **[55]**:

$$H_v = 0.92(G/B)^{1.137} G^{0.708} \quad (21)$$

The values of H_v in α-Bi_2O_3 at 0 GPa in the Voigt, Reuss and Hill approximations are included in **Table 1**. Bismite has a value of H_v = 4.90 GPa at 0 GPa in the Hill approximation. Consequently, this sequioxide can be considered as a relatively soft material because H_v is smaller than 10 GPa. The soft behavior of α-Bi_2O_3 is related with its ductile behavior at 0 GPa, as previously shown.

Finally, we have calculated the average sound velocity, v_m, in α-Bi_2O_3 from the known elastic moduli **[56]**. This velocity is a quantity which provides information on the elastic moduli, elastic anisotropy, and other thermodynamic properties. In polycrystalline materials v_m can be obtained by the expression **[57]**:

$$v_m = \left[\frac{1}{3} \left(\frac{2}{v_{trans}^3} + \frac{1}{v_{lon}^3} \right) \right]^{-1/3} \quad (22)$$

In **Eq. 22**, v_{trans} and v_{lon} are the transverse and longitudinal elastic wave velocities of the polycrystalline material:

$$v_{lon} = \left(\frac{B + \frac{4}{3} G}{\rho} \right)^{1/2} \quad (23)$$

$$v_{trans} = \left(\frac{G}{\rho} \right)^{1/2} \quad (24)$$

where ρ is the density of the material and B and G are the elastic moduli. **Table 5** shows the density and wave velocities v_m, v_{lon} and v_{trans} in α-Bi_2O_3 at 0 GPa. The obtained value of v_m in the Hill approximation (2088.8 m/s) at 0 GPa is similar to that obtained for porous α-Bi_2O_3 (v_m = 2111±432 m/s) in shock compression experiments **[8]**, and

39% smaller than that obtained by the calculated Hugoniot for bulk α-Bi_2O_3 (v_m = 3432 m/s) in dynamic experiments **[8]**.

b) At high pressure

The HP evolution of the elastic constants, C_{ij}, and of the elastic stiffness coefficients, B_{ij}, in α-Bi_2O_3 are given in **Figs. 3 and 4**, respectively. We report the HP dependence of B_{ij} and C_{ij}, although only B_{ij} are valid at any pressure, because B_{ij} are obtained from the C_{ij}. As it can be observed, B_{11}, B_{22}, B_{33}, B_{12}, B_{13}, B_{15} and B_{23} (B_{55} and B_{35}) increase (decrease) with pressure in the whole pressure range studied. However, B_{44}, B_{66}, B_{25} and B_{46} increase with pressure up to 4.5, 15.5, 11.2 and 10.3 GPa, respectively, and then decrease as pressure increases. It must be noted that B_{35} changes its sign at 14.0 GPa.

From the HP dependence of the elastic stiffness coefficients, the HP evolution of the B, G, and E elastic moduli, ν Poisson's ratio, and B/G ratio for α-Bi_2O_3 is calculated (**Fig. 5**). For the sake of simplicity, only the HP dependence of the elastic moduli in the average Hill approximation will be commented. As it can be seen, B_H increases under compression, reaches a maximum value of 118.3 GPa at 12.6 GPa, and then it decreases under pressure. Similarly, E_H increases with pressure achieving a maximum value of 87.3 at 1.6 GPa and decreases above that pressure. In turn, G_H decreases with pressure in the whole pressure range studied. Finally, ν also increases with pressure, reaching a value of 0.42 at 18.1 GPa. It must be stressed that the HP increase of ν indicates that the ductility and the metallic behavior increase under compression. This metallization can be understood as a decrease of the ionic character of the material. In this sense, the effect of pressure on bismite is the increase of atomic coordination and progressive reduction of interatomic bond directionality. We note that bond directionality decreases in the sequence covalent-ionic-metallic of bond character.

It can also be observed that the *B/G* ratio increases at HP in α-Bi_2O_3, reaching a value of 6.1 at 18.1 GPa. Since the *B/G* ratio is related to the Poisson's ratio **[49]**, the increase in *B/G* also indicates an increment of the ductility under compression.

Figure 6 shows the evolution with pressure of the different anisotropy indexes previously defined for bismite. The compression and shear anisotropy factors (A_B, A_G), A_3 shear anisotropy factor, and A_U universal anisotropy factor increase significantly under compression. This denotes a considerable increment of the elastic anisotropy in α-Bi_2O_3 with pressure. On the other hand, A_1 and A_2 shear anisotropy factors have a small variation with pressure.

Figure 7 presents the HP dependence of the Vickers hardness in α-Bi_2O_3. Clearly, H_v decreases as pressure increases because the *G* elastic modulus and, consequently, the *G/B* ratio decrease with pressure. Therefore, bismite becomes softer as pressure increases; a result which is related to the increase of its ductility (*B*/*G* ratio), as previously commented.

The HP dependence of the sound velocities for α-Bi_2O_3 is given in **Figure 8**. The calculated v_{lon}, obtained with elastic moduli in the Hill approximation, increases with pressure reaching a maximum value of 3761.7 m/s at 9.7 GPa and decreases above that pressure. Moreover, the calculated velocities v_{trans} and v_m in all approximations decrease as pressure increases, thus reflecting the decrease of *G*.

It must be stressed that the crystalline structure of a compound in a given structure is stable if it is mechanically and dynamically stable **[58-60].** Taking into account that we have evaluated the mechanical stability of bismite at room pressure in section 3.1.a) through the Born stability criteria, and that bismite is also dynamically stable at room pressure **[23]**, now we evaluate in this section the mechanical stability of bismite at HP on the basis of the theoretically calculated elastic constants at HP.

When a non-zero stress is applied to the crystal, a generalization of the Born stability criteria is required **[61, 62]**. The generalized Born stability criteria for monoclinic crystals are obtained by replacing in **Eqs. 1-6** the C_{ij} elastic constants by the B_{ij} elastic stiffness coefficients. These criteria are given by:

$$M_1 = B_{11} > 0 \tag{25}$$

$$M_2 = B_{11}B_{22} - B_{12}^2 > 0 \tag{26}$$

$$M_3 = (B_{22}B_{33} - B_{23}^2)B_{11} - B_{33}B_{12}^2 + 2B_{23}B_{12}B_{13} - B_{22}B_{13}^2 > 0 \tag{27}$$

$$M_4 = B_{44} > 0 \tag{28}$$

$$\begin{aligned} M_5 = {} & B_{12}^2B_{35}^2 - B_{33}B_{55}B_{12}^2 + 2B_{55}B_{12}B_{13}B_{23} - 2B_{12}B_{13}B_{25}B_{35} \\ & - 2B_{12}B_{15}B_{23}B_{35} + 2B_{33}B_{12}B_{15}B_{25} + B_{13}^2B_{25}^2 - B_{22}B_{55}B_{13}^2 \\ & - 2B_{13}B_{15}B_{23}B_{25} + 2B_{22}B_{13}B_{15}B_{35} + B_{15}^2B_{23}^2 - B_{22}B_{33}B_{15}^2 \\ & - B_{11}B_{55}B_{23}^2 + 2B_{11}B_{23}B_{25}B_{35} - B_{11}B_{33}B_{25}^2 - B_{11}B_{22}B_{35}^2 \\ & + B_{11}B_{22}B_{33}B_{55} > 0 \end{aligned} \tag{29}$$

$$M_6 = B_{44}B_{66} - B_{46}^2 > 0 \tag{30}$$

Figure 9 reports the evolution of the generalized stability criteria in α-Bi_2O_3 under compression. At HP up to 23 GPa, all stability criteria are satisfied except M_5 (**Eq. 29**), which is violated at 19.3 GPa. Therefore, our simulations show that α-Bi_2O_3 becomes mechanically unstable above 19.3 GPa. This value is consistent with the quick increase of the A_B, A_G and A_U anisotropy factors above 16 GPa in α-Bi_2O_3 (see **Figure 6**), which is typically observed when a compound approaches the mechanical instability **[63]**.

3.2. Dynamical stability of bismite

In this section, we will focus on the study of the dynamical stability of the monoclinic structure of α-Bi_2O_3 at HP. For that purpose, we have performed lattice dynamics calculations and have evaluated the PDC at different pressures (see **Figure 10**). It can be observed that our calculations do not show any phonon branch with imaginary frequencies at any point of the BZ in α-Bi_2O_3 at 0 GPa in good agreement with a previous report **[23]**. Therefore, bismite is dynamically stable at room pressure as previously commented. However, imaginary frequencies (below 0 in the ordinate scale of **Figure 10**) are developed above 11.5 GPa. Therefore, our theoretical calculations predict that bismite becomes dynamically unstable at HP (above 11.5 GPa) before becoming mechanically unstable (above 19.3 GPa).

To conclude this section, we want to comment that our results on the mechanical and dynamical stability of bismite at HP allow us to understand previous works that have studied the behavior of Bi_2O_3 under compression **[16, 22, 23, 64, 65].** In this context, a phase transition was predicted to occur around 5.5 GPa from the monoclinic α-Bi_2O_3 phase to the hexagonal HPC-Bi_2O_3 phase **[64]**. However, this phase transition was not observed experimentally at room temperature, probably due to the hindrance of the pressure-driven phase transition at room temperature. Additionally, a pressure-induced amorphization of α-Bi_2O_3 was observed between 15 and 20 GPa depending on the hydrostatic conditions **[16, 22, 23]**. Noteworthy, the experimental amorphization of α-Bi_2O_3 under compression is consistent with the results of the present theoretical study of the mechanical and dynamical stability of α-Bi_2O_3 which suggest that amorphization could be caused by the dynamical and mechanical instabilities theoretically predicted to occur on α-Bi_2O_3 under purely hydrostatic pressure above 11.5 and 19.3 GPa, respectively. The difference between experimental and theoretical pressure values for the onset of the pressure-induced amorphization could be ascribed to the non-purely

hydrostatic compression of α-Bi_2O_3 in the reported experiments, which could favour a larger stability of the monoclinic phase **[16, 22, 23]**.

3.3. Thermodynamic properties of bismite

To conclude this work, we want to calculate some thermodynamic properties of bismite, such as the Debye temperature and the minimum thermal conductivity, from the knowledge of the average sound velocity, v_m. The Debye temperature, θ_D, corresponds to the upper limit of phonon frequency in a crystal lattice and it can be calculated with the semi-empirical formula **[57]**:

$$\theta_D = \frac{h}{k_B}\left[\frac{3n}{4\pi}\left(\frac{N_A\rho}{M}\right)\right]^{1/3} v_m \quad (31)$$

In **Eq. 31** h is the Planck's constant, k_B is the Boltzmann's constant, n is the number of atoms in the molecule, N_A is the Avogadro's number, ρ is the density, M is the molecular weight, and v_m is the average sound velocity. The value of θ_D = 245.7 K in the Hill approximation, for α-Bi_2O_3 at 0 GPa (see **Table 5**), is 22% smaller than the estimated value of θ_D = 316 K, obtained from shock compression data using Lindemman's melting law **[8]**. A decrease of θ_D with pressure, clearly following the decrease of v_m with pressure, is observed in bismite (see **Fig. 11(a)**).

On the other hand, the thermal conductivity is a property that allows modeling the heat transfer in solids. The theoretical minimum of the thermal conductivity has been estimated by using the expression given by Clarke **[66]**:

$$\kappa_{min} = k_B v_m \left(\frac{M}{n\rho N_A}\right)^{-2/3} \quad (32)$$

and the expression given in Long's model [**67**]:

$$\kappa_{\min} = \left\{ \frac{1}{3} \left[2(2+2\nu)^{\frac{3}{2}} + \left(1 - \frac{2\nu^2}{1-\nu} \right)^{\frac{3}{2}} \right] \right\}^{-\frac{1}{3}} \cdot k_B m^{\frac{2}{3}} \cdot \left(\frac{E}{\rho} \right)^{\frac{1}{2}} \quad (33)$$

where m is the number of atoms per volume. Both expressions give the same result for $\kappa_{\min}$ and take into account the anisotropic elasticity of monoclinic α-Bi_2O_3. The value of $\kappa_{\min}$ in the Hill approximation, for α-Bi_2O_3 at 0 GPa, is 0.45 W m^{-1} K^{-1} (see **Table 5**). Therefore, this sesquioxide can be considered as a low κ material interesting for thermoelectric applications **[68]**. As shown in **Figure 11(b)**, $\kappa_{\min}$ in the Hill approximation increases slightly as pressure increases from 0 to 1.6 GPa and then decreases as pressure increases. It should be stressed that the calculated value of $\kappa_{\min}$ = 0.45 W m^{-1} K^{-1} is smaller than the thermal conductivity measured at room temperature for α-Bi_2O_3 which turns out to be 1.3 W m^{-1} K^{-1} **[69]**. Therefore, we consider that there is room for improvement in the decrease of the thermal conductivity of bismite both at room pressure and at HP conditions for thermoelectric applications **[70]**.

4. Conclusions

In the present work, the elastic and thermodynamic behavior of α-Bi_2O_3 has been studied theoretically both at room pressure and under hydrostatic compression. The values at room pressure and the HP dependence of the elastic moduli, Poisson's ratio, *B/G* ratio and elastic anisotropy indexes of bismite are reported as well as a study of the directional dependence of Young modulus and linear compressibility at 0 GPa.

Our results show that this sesquioxide: i) is ductile at all pressures and has a larger resistance to volume compression than to shear deformation; ii) shows an intrinsic elastic anisotropy which increases with pressure; iii) is relatively soft at room

pressure and its hardness decreases under compression. Besides, its average sound velocity and Debye temperature decrease with increasing pressure. Moreover, we have found that α-Bi_2O_3 is a material with a very low thermal conductivity that could be useful for thermoelectric applications both at low and high pressures.

Finally, the study of the mechanical and dynamical stability of the monoclinic structure of bismuth oxide at high pressure shows that this structure becomes mechanically and dynamically unstable above 19.3 and 11.5 GPa, respectively. This result indicates that amorphization of α-Bi_2O_3, found experimentally between 15 and 20 GPa, could be due to the dynamical and mechanical instabilities of this monoclinic phase. We hope that the current theoretical work on bismite will stimulate experimental studies of its elastic and thermodynamic properties.

Acknowledgements

This research was supported by the Spanish Ministerio de Economía y Competitividad under Projects MAT2016-75586-C4-2-P/3-P and MAT2015-71070-REDC. P.R.-H. and A.M. acknowledge Red Española de Supercomputación (RES) and MALTA-Cluster for the computing time.

References

[1] N. M. Sammes, G. A. Tompsett, H. Näfe, F. Aldinger, J. Eur. Ceram. Soc. 19 (1999) 1801–1826.

[2] H. A. Harwig, Z. Anorg. Allg. Chem. 444 (1978) 151-166.

[3] L. Zhou, W. Wang, H. Xu, S. Sun, M. Shang, Chem. Eur. J. 15 (2009) 1776-1782.

[4] Z. Ai, Y. Huang, S. Lee, L. Zhang, J. Alloy Comp. 509 (2011) 2044-2049.

[5] S. Iyyapushpam, S. T. Nishanthi, D. Pathinettam Padiyan, Mater. Lett. 86 (2012) 25-27.

[6] A. Cabot, A. Marsal, J. Arbiol, J. R. Morante, Sensor. Actuator. B 99 (2004) 74-89.

[7] F. L. Zheng, G. R. Li, Y. N. Ou, Z. L. Wang, C. Y. Su, Y. X. Tong, Chem. Commun. 46 (2010) 5021-5023.

[8] D. A. Fredenburg, N. N. Thadhani, J. Appl. Phys. 110 (2011) 063510.

[9] E. A. Kravchenko, V. G.Orlov, Z. Naturforsch. 49a (1994) 418-424.

[10] A . I . Kharkovskii, V. I. Nizhankovskii, E. A. Kravchenko, V. G. Orlov, Z. Naturforsch. 51 (1996) 665-666.

[11] V. G. Orlov, A. A. Bush, S. A. Ivanovt, V. V. Zhurovt, J. Low Temp. Phys. 105 (1996) 1541-1546.

[12] A. Walsh, G. W. Watson, D. J. Payne, R. G. Edgell, J. Guo, P. A. Glans, T. Learmonth, K. E. Smith, Phys. Rev. B 73 (2006) 235104.

[13] V. Dolocan, F. Iova, phys. stat. sol. (a) 64 (1981) 755-759.

[14] O. M. Bordun, I. I. Kukharskii, V. V. Dmitruk, V. G. Antonyuk, V. P. Savchin, J. Appl. Spectrosc. 75 (2008) 681-684.

[15] M. Yashima, D. Ishimura, K. Ohoyama, J. Am. Ceram. Soc. 88 (2005) 2332–2335.

[16] A. L. J. Pereira, D. Errandonea, A. Beltrán, L. Gracia, O. Gomis, J. A. Sans, B. García-Domene, A. Miquel-Veyrat, F. J. Manjón, A. Muñoz, C. Popescu, J. Phys.: Condens. Matter 25 (2013) 475402.

[17] R. J. Betsch, W. B. White, Spectrochimica Acta A 34 (1978) 505-514.

[18] A. Crossley, P. R. Graves, S. Myhra, Physica C 176 (1991) 106-112.

[19] S. N. Narang, N. D. Patel, V. B. Kartha, J. Mol. Struct. 327 (1994) 221-235.

[20] A. B. Kuz'menkoy, E. A. Tishchenkoy, V G Orlov, J. Phys.: Condens. Matter 8 (1996) 6199–6212.

[21] V. N. Denisov, A .N. Ivlevy, A. S. Lipiny, B. N. Mavriny, V. G. Orlovz, J. Phys.: Condens. Matter 9 (1997) 4967–4978.

[22] C. Chouinard, S. Desgreniers, Solid State Commun. 113 (2000) 125–129.

[23] A. L. J. Pereira, O. Gomis, J. A. Sans, J. Pellicer-Porres., F. J. Manjón, A. Beltran, P. Rodríguez-Hernández, A. Muñoz, J. Phys.: Condens. Matter 26 (2014) 225401.

[24] P. Hohenberg, W. Kohn, Phys. Rev. 136 (1964) B864-B871.

[25] G. Kresse, J. Hafner, Phys. Rev. B 47 (1993) 558-561; G. Kresse, J. Hafner, Phys. Rev. B 49 (1994) 14251-14269; G. Kresse, J. Furthmüller, Comput. Mat. Sci. 6 (1996) 15-50; G. Kresse, J. Furthmüller, Phys. Rev. B 54 (1996) 11169-11186.

[26] P. E. Blöchl, Phys. Rev. B 50 (1994) 17953-17959; G. Kresse, D. Joubert, Phys. Rev. B 59 (1999) 1758-1775.

[27] J. P. Perdew, A. Ruzsinszky, G. I. Csonka, O. A. Vydrov, G. E. Scuseria, L. A. Constantin, X. Zhou, K. Burke, Phys. Rev. Lett. 100 (2008) 136406.

[28] A. Mujica, A. Rubio, A. Muñoz, R. J. Needs, Rev. Mod. Phys. 79 (2003) 863-912.

[29] K. T. Jacob, A. K. Mansoor, Thermochimica Acta 630 (2016) 90-96.

[30] O. H. Nielsen, R. M. Martin, Phys. Rev. B 1985, 32, 3780–3791.

[31] N. Chetty, A. Muñoz, R. M. Martin, Phys. Rev. B 40 (1989) 11934-11936.

[32] Y. Le Page, P. Saxe, Phys. Rev. B 65 (2002) 104104.

[33] O. Beckstein, J. E. Klepeis, G. L. W. Hart, O. Pankratov, Phys. Rev. B 63 (2001) 134112.

[34] K. Parlinsky, Computer Code PHONON. http://wolf.ifj.edu.pl/phonon/, 2008 (accessed 08 May 2018).

[35] K. Parlinsky, Z. Q. Li, Y. Kawazoe, Phys. Rev. Lett. 78 (1997) 4063.

[36] J. F. Nye, Physical properties of crystals. Their representation by tensor and matrices, Oxford University Press, 1957.

[37] D. C. Wallace, Thermoelastic Theory of Stressed Crystals and Higher-Order Elastic Constants, in: F.S. Henry Ehrenreich, D. Turnbull, F. Seitz (Eds.), Solid State Physics, vol. 25, Academic Press, 1970, pp. 301–404.

[38] J. Philip, N. Rodrigues, M. Sadhukan, A. K. Bera, B. K. Chaudhuri, J. Mat. Sci. 35 (2000) 229-233.

[39] D. Ma, A. D. Stoica, X. L. Wang, Z. P. Lu, B. Clausen, D. W. Brown, Phys. Rev. Lett. 108 (2012) 085501.

[40] M. Born, K. Huang, Dynamical Theory of Crystal Lattices, Oxford University Press, London, 1954, p. 140.

[41] X. S. Zhao, S. L. Shang, Z. K. Liu, J. Y. Shen, J. Nucl. Mat. 415 (2011) 13-17.

[42] W. Voigt, Lehrbstch der Kristaltphysih, B. G. Teubner, Leipzig, Germany, 1928.

[43] A. Reuss, Z. Angew, Math. Mech. 9 (1929) 49-58.

[44] R. Hill, Proc. Phys. Soc. London A 65 (1952) 349-354.

[45] O. Gomis, D. Santamaría-Pérez, J. Ruiz-Fuertes, J. A. Sans, R. Vilaplana, H. M. Ortiz, B. García-Domene, F. J. Manjón, D. Errandonea, P. Rodríguez-Hernández, A. Muñoz, M. Mollar, J. Appl. Phys. 116 (2014) 133521.

544 [46] R. J. Angel, J. L. Mosenfelder, C. S. J. Shaw, Phys. Earth Planet Inter. 124 (2001)
545 71-79.
546 [47] P. Ravindran, L. Fast, P. A. Korzhavyi, B. Johansson, J. Wills, O. Eriksson, J.
547 Appl. Phys. 84 (1998) 4891-4904.
548 [48] V. V. Brazhkin, A. G. Lyapin, R. J. Hemley, Philos. Mag. A 82 (2002) 231-253.
549 [49] G. N. Greaves, A. L. Greer, R. S. Lakes, T. Rouxel, Nat. Mater. 10 (2011) 823-
550 837.
551 [50] S. F. Pugh, Philos. Mag. 45 (1954) 823-843.
552 [51] V. Tvergaard, J. W. Hutchinson, J. Am. Ceram. Soc. 71 (1988) 157-166.
553 [52] D. Connétable, O. Thomas, Phys. Rev. B 79 (2009) 094101.
554 [53] S.I. Ranganathan, M. Ostoja-Starzewski, Phys. Rev. Lett. 101 (2008) 055504.
555 [54] R. Gaillac, P. Pullumbi, F. X. Coudert, J. Phys.: Condens. Matter 28 (2016)
556 275201.
557 [55] Y. Tian, B. Xu, Z. Zhao, Int. J. Refract. Met. H. 33 (2012) 93-106.
558 [56] J. P. Poirier, Introduction to the Physics of the Earth's Interior, Cambridge
559 University Press, Cambridge, 2000.
560 [57] O. L. Anderson, J. Phys. Chem. Solids 24 (1963) 909-917.
561 [58] P. Goel, R. Mittal, N. Choudhury, S. L. Chaplot, J. Phys.: Condens. Matter 22
562 (2010) 065401.
563 [59] A. V. Lugovskoy, M. P. Belov, Yu. Kh. Velikov, O.M. Krasilnikov, J. Phys.: Conf.
564 Ser. 490 (2014) 012059.
565 [60] O. Gomis, B. Lavina, P. Rodríguez-Hernández, A. Muñoz, R. Errandonea,
566 D. Errandonea, M. Bettinelli, J. Phys.: Condens. Matter 29 (2017) 095401.
567 [61] J. Wang, S. Yip, S. R. Phillpot, D. Wolf, Phys. Rev. Lett. 71 (1993) 4182-4185.

[62] G. Grimvall, B. Magyari-Köpe, V. Ozolinš, K. A. Persson, Rev. Mod. Phys. 84 (2012) 945-986.

[63] O. Gomis, H. M. Ortiz, J. A. Sans, F. J. Manjón, D. Santamaría-Pérez , P. Rodríguez-Hernández, A. Muñoz, J. Phys. Chem. Solids 98 (2016) 198-208.

[64] A. L. J. Pereira, O. Gomis, J. A. Sans, J. Contreras-García, F. J. Manjón, P. Rodríguez-Hernández, A. Muñoz, A. Beltran, Phys. Rev. B 93 (2016) 224111.

[65] T. Locherer, D. L. V. K. Prasad, R. Dinnebier, U. Wedig, M. Jansen, G. Garbarino, T. Hansen, Phys. Rev. B 83 (2011) 214102.

[66] D. R. Clarke, Surface and Coatings Technology 163 (2003) 67-74.

[67] H. Chen, W. Tian, Physica B 524 (2017) 144-148.

[68] C. G. Levi, Curr. Opin. Solid St. M. 8 (2004) 77-91.

[69] N. I. Anisimova, G. A. Bordovsky, V. A. Bordovsby, V. I. Seldayev, Proceedings of the 2004 IEEE International Conference on Solid Dielectrics, 2004. 5-9 July 2004. Toulouse, France. doi: 10.1109/ICSD.2004.1350310.

[70] J. H. Eom, H. J. Jung, J. H. Han, J. Y. Lee, S. G. Yoon, ECS Journal of Solid State Science and Technology 3 (2014) 315-319.

589 **Table 1.** C_{ij} elastic constants (in GPa) for α-Bi_2O_3. Elastic moduli B, G, and E (in GPa),
590 Possion's ratio (ν), B/G ratio, and Vickers hardness (H_v in GPa) are obtained in the
591 Voigt, Reuss and Hill approximations, labeled respectively with subscripts V, R, and H.
592 The percentage of anisotropy in both compression (A_B) and shear (A_G), as well as the
593 shear anisotropic factors (A_1, A_2, A_3) and the universal anisotropy index (A_U) are also
594 included. Data are calculated at 0 GPa.

	α-Bi_2O_3[a]
C_{11}	114.0
C_{12}	59.1
C_{13}	57.1
C_{15}	10.2
C_{22}	84.3
C_{23}	30.4
C_{25}	2.6
C_{33}	150.3
C_{35}	10.5
C_{44}	30.0
C_{46}	8.3
C_{55}	36.4
C_{66}	46.4
B_V, B_R, B_H	71.3, 65.3, 68.3
G_V, G_R, G_H	36.0, 30.9, 33.4
E_V, E_R, E_H	92.5, 80.0, 86.3
ν_V, ν_R, ν_H	0.28, 0.30, 0.29
B_V/G_V, B_R/G_R, B_H/G_H	1.98, 2.12, 2.04
A_B (%), A_G (%), A_1, A_2, A_3, A_U	4.35, 7.73, 0.80, 0.84, 2.32, 0.93
H_v (V, R, H)	5.36, 4.44, 4.90

595 [a] Our *ab initio* calculations.

596 **Table 2.** Born stability conditions in α-Bi_2O_3 at 0 GPa.

597

m_1 (GPa)	114.0
m_2 (GPa^2)	$61.1 \cdot 10^2$
m_3 (GPa^3)	$74.4 \cdot 10^4$
m_4 (GPa)	30.0
m_5 (GPa^4)	$261.4 \cdot 10^5$
m_6 (GPa^2)	$13.2 \cdot 10^2$

598

599

600 **Table 3.** Axial compressibilities, κ_a, κ_b and κ_c, in α-Bi_2O_3 obtained from the elastic
601 constants at 0 GPa. The axial compressibilities reported in **Ref 16,** obtained from a
602 Murnaghan equation of state fit of data, are also given for comparison.

603

κ_a (10^{-3} GPa^{-1})	κ_b (10^{-3} GPa^{-1})	κ_c (10^{-3} GPa^{-1})	
2.36	8.79	4.15	This work
1.53(1)	7.84(2)	2.50(1)	**Ref 16**
2.07(1)	6.64(1)	4.41(1)	**Ref 16**

604
605

606 **Table 4.** Maximum and minimum values for the Young modulus, E, and linear
607 compressibility, κ. The anisotropy ratio (maximum value/minimum value) and direction
608 of minimum and maximum value for E and κ are also included. Data are calculated at 0
609 GPa with the ELATE software **[54]**.
610

	Young modulus (GPa)		Linear compressibility (TPa^{-1})	
	E_{min}	E_{max}	κ_{min}	κ_{max}
value	53.4	127.0	1.7	8.8
anisotropy ratio	2.4		5.1	
direction of minimum and maximum value[a]	(0, 1, 0)	(0.30, 0, 0.95)	(0.89, 0, 0.45)	(0, 1, 0)

611

612 [a] in Cartesian coordinates (x, y, z).
613

614 **Table 5.** Density (ρ in g/cm^3), longitudinal (v_{lon}), transverse (v_{trans}) and averaged (v_m)
615 elastic wave velocity (in m/s), Debye temperature (θ_D in K), and minimum thermal
616 conductivity (κ_{min} in W m^{-1} K^{-1}) in α-Bi_2O_3 at 0 GPa. The labels *V, R,* and *H* refer to the
617 Voigt, Reuss and Hill approximations, respectively.
618

ρ	9.539
v_{lon} (V, R, H)	3537.0, 3341.3, 3440.5
v_{trans} (V, R, H)	1943.6, 1798.7, 1872.5
v_m (V, R, H)	2166.5, 2008.1, 2088.8
θ_D (V, R, H)	254.8, 236.2, 245.7
κ_{min} (V, R, H)	0.47, 0.43, 0.45

619
620

621 **Figure captions**

622

623 **Figure 1.** (**Color online**) Crystalline structure for α-Bi_2O_3. Large (blue) spheres
624 represent Bi atoms and small (red) spheres O atoms.

625 **Figure 2. (Color online)** (left) Directional dependence of the Young modulus, in units
626 of GPa, and (right) spatial dependence of the linear compressibility, in units of TPa^{-1}, in
627 bismite at 0 GPa. The Young modulus and linear compressibility in a given direction
628 are shown as a green surface. Data plotted with the ELATE software **[54]**.

629 **Figure 3.** (**Color online**) Theoretical pressure evolution of the elastic constants, C_{ij}, in
630 α-Bi_2O_3. Solid lines connecting the calculated data points are guides to the eyes.

631 **Figure 4. (Color online)** Theoretical pressure evolution of the elastic stiffness
632 coefficients, B_{ij}, in α-Bi_2O_3. Solid lines connecting the calculated data points are guides
633 to the eyes.

634 **Figure 5**. **(Color online)** Pressure evolution of the elastic moduli (B, G, and E),
635 Poisson's ratio (ν), and B/G ratio in α-Bi_2O_3. The results are given in the Voigt
636 (squares), Reuss (circles), and Hill (triangles) approximations. Solid lines connecting
637 the calculated data points are guides to the eyes.

638 **Figure 6. (Color online)** Pressure evolution of the percentage elastic anisotropy in both
639 compression (A_B) and shear (A_G), shear anisotropic factors (A_1, A_2, A_3) and universal
640 anisotropy index (A_U). Solid lines connecting the calculated data points are guides to the
641 eyes.

642 **Figure 7. (Color online)** Pressure dependence of the Vickers hardness (H_V) in α-Bi_2O_3.
643 The results are given in the Voigt (squares), Reuss (circles), and Hill (triangles)
644 approximations. Solid lines connecting the calculated data points are guides to the eyes.

645 **Figure 8. (Color online)** Pressure dependence of the longitudinal (v_{lon}), transverse
646 (v_{trans}), and average (v_m) elastic wave velocity in α-Bi_2O_3. The results are given in the
647 Voigt (squares), Reuss (circles), and Hill (triangles) approximations. Solid lines
648 connecting the calculated data points are guides to the eyes.

649 **Figure 9. (Color online)** General Born stability criteria in α-Bi_2O_3. P_{mu} reports the
650 pressure at which α-Bi_2O_3 becomes mechanically unstable. Solid lines connecting the
651 calculated data points are guides to the eyes.

652 **Figure 10.** (**Color online**) Phonon dispersion curves in α-Bi_2O_3 at (a) 0 GPa and (b)
653 11.5 GPa.

654 **Figure 11. (Color online)** Evolution with pressure of (a) the Debye temperature (θ_D),
655 and (b) the minimum thermal conductivity (κ_{min}) in α-Bi_2O_3. The results are given in
656 the Voigt (squares), Reuss (circles), and Hill (triangles) approximations. Solid lines
657 connecting the calculated data points are guides to the eyes.

658

659

660 **Figure 1**

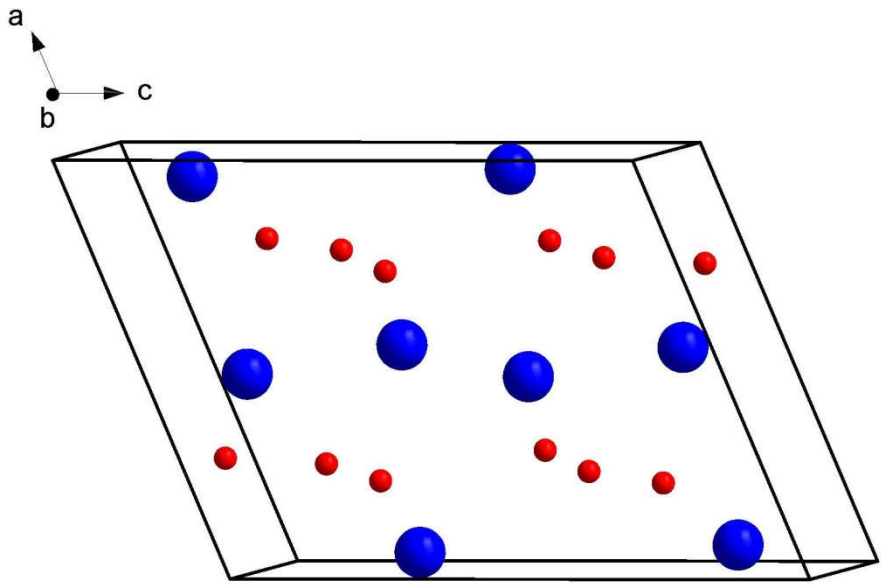

661
662

663 **Figure 2**

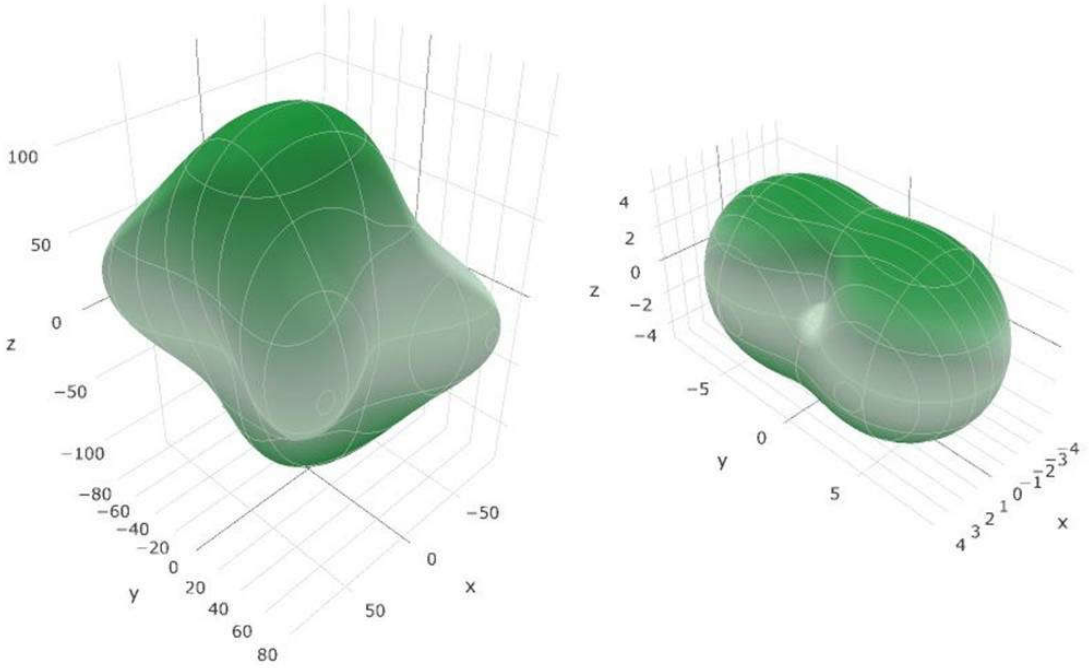

664

665

Figure 3

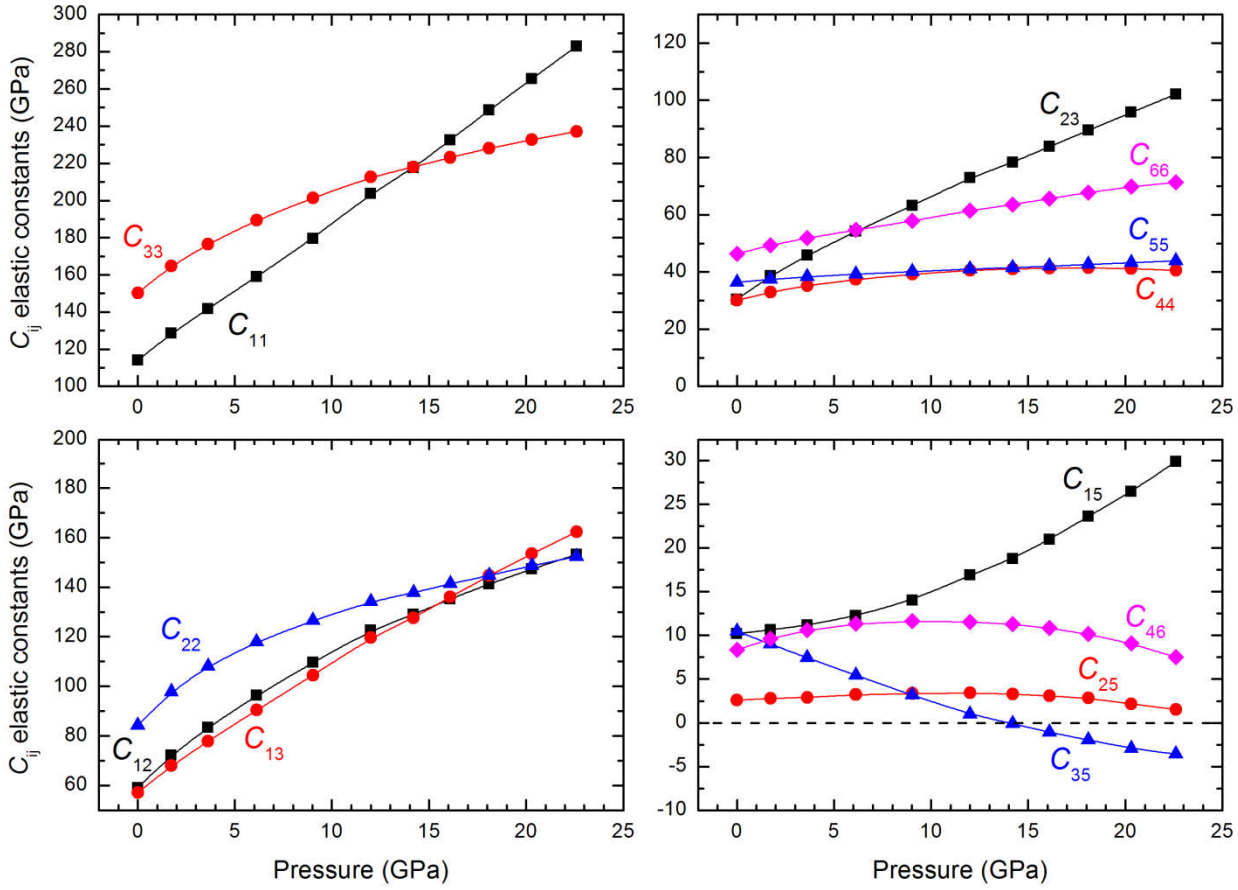
C_ij elastic constants (GPa)
C33
C11
C23
C66
C55
C44
C22
C12
C13
C15
C46
C25
C35
Pressure (GPa)
Pressure (GPa)

669 **Figure 4**

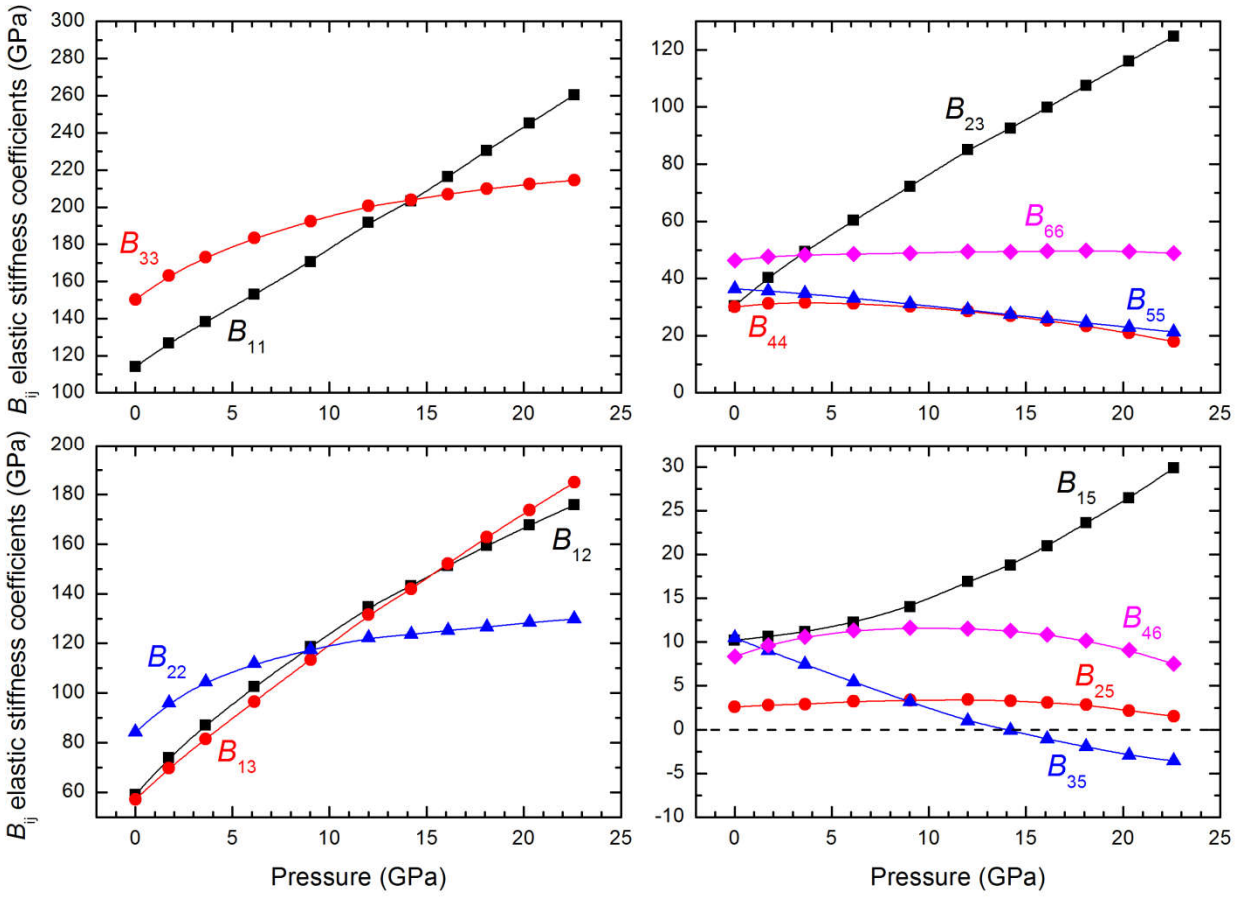

670

671

672

673 **Figure 5**

674

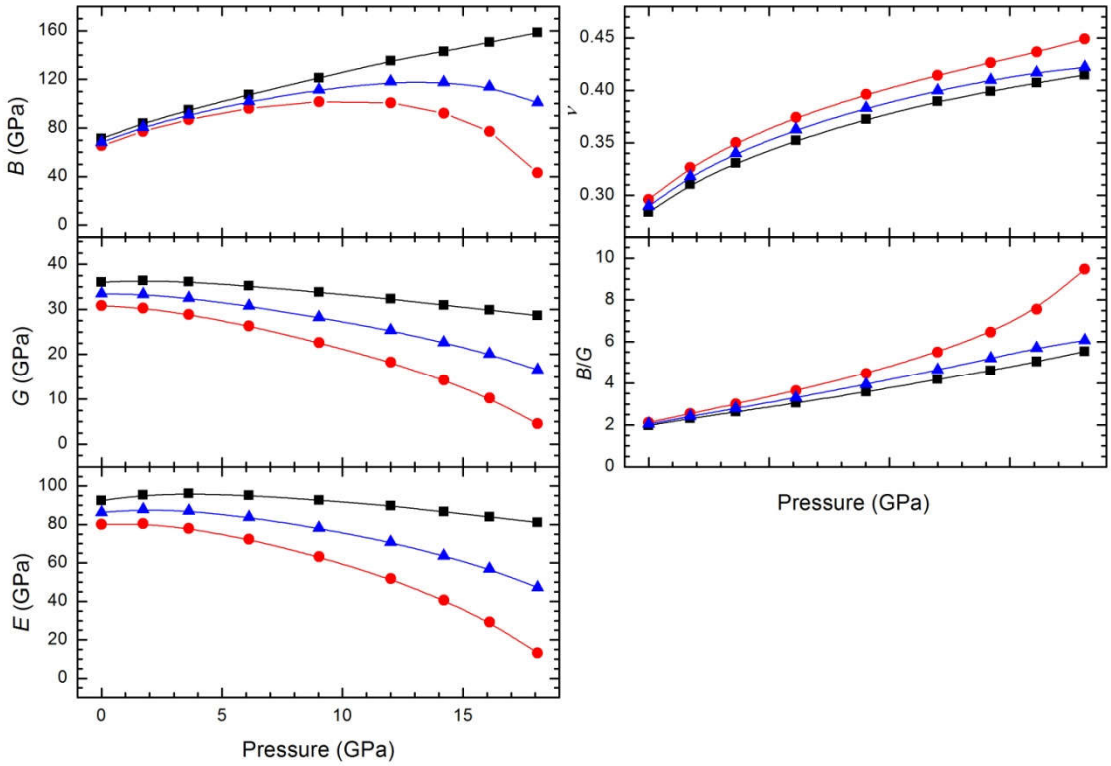

675
676

677

678

679

Figure 6

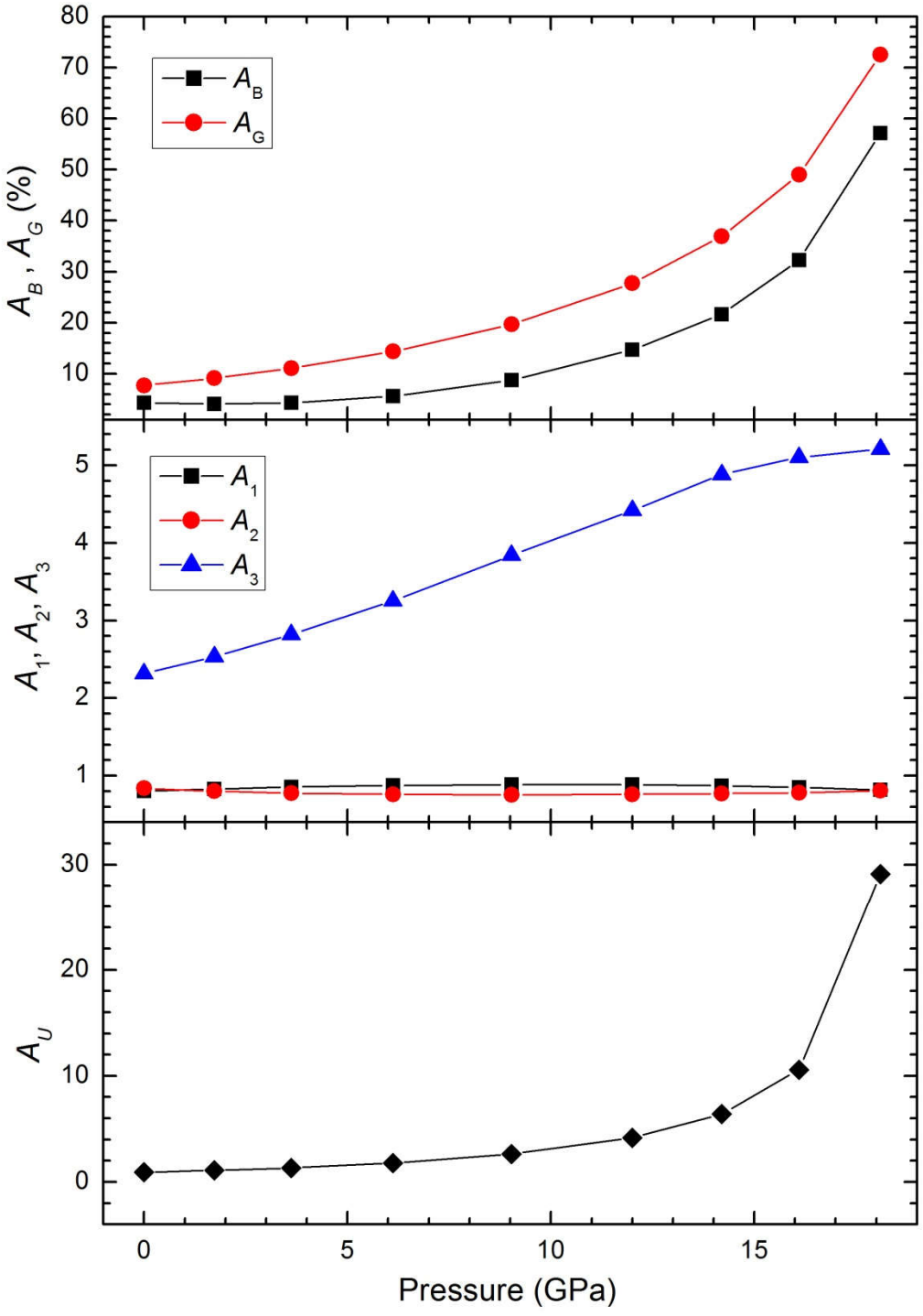

689 **Figure 7**
690

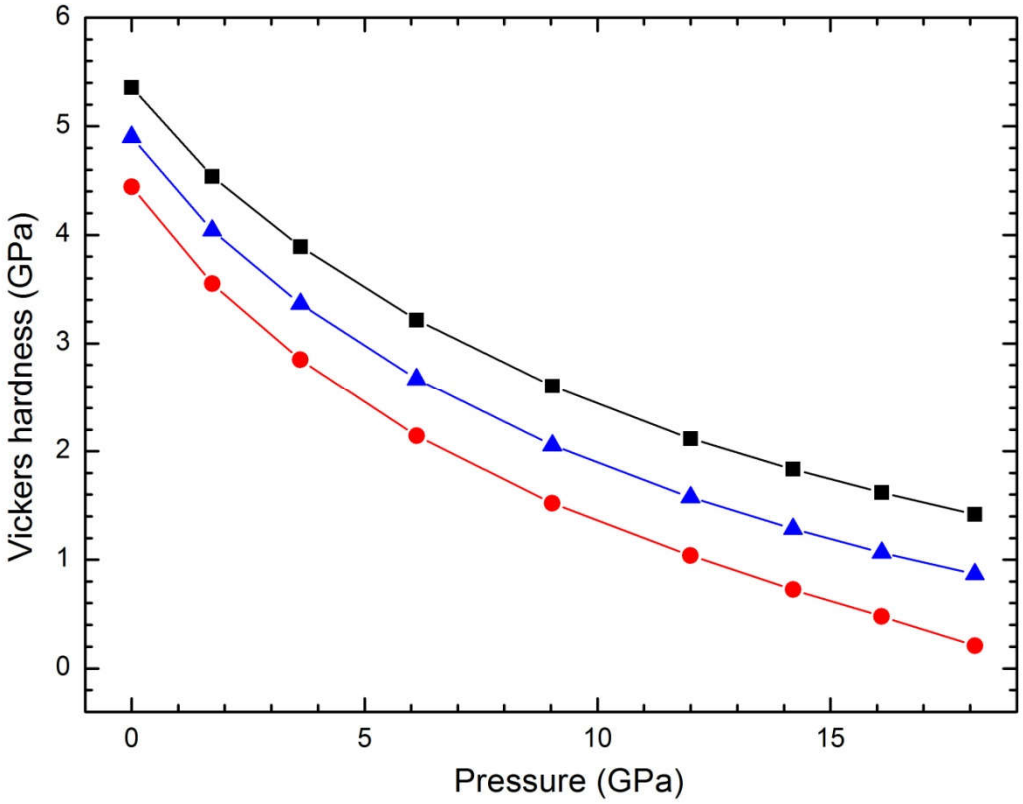

691
692

693 **Figure 8**

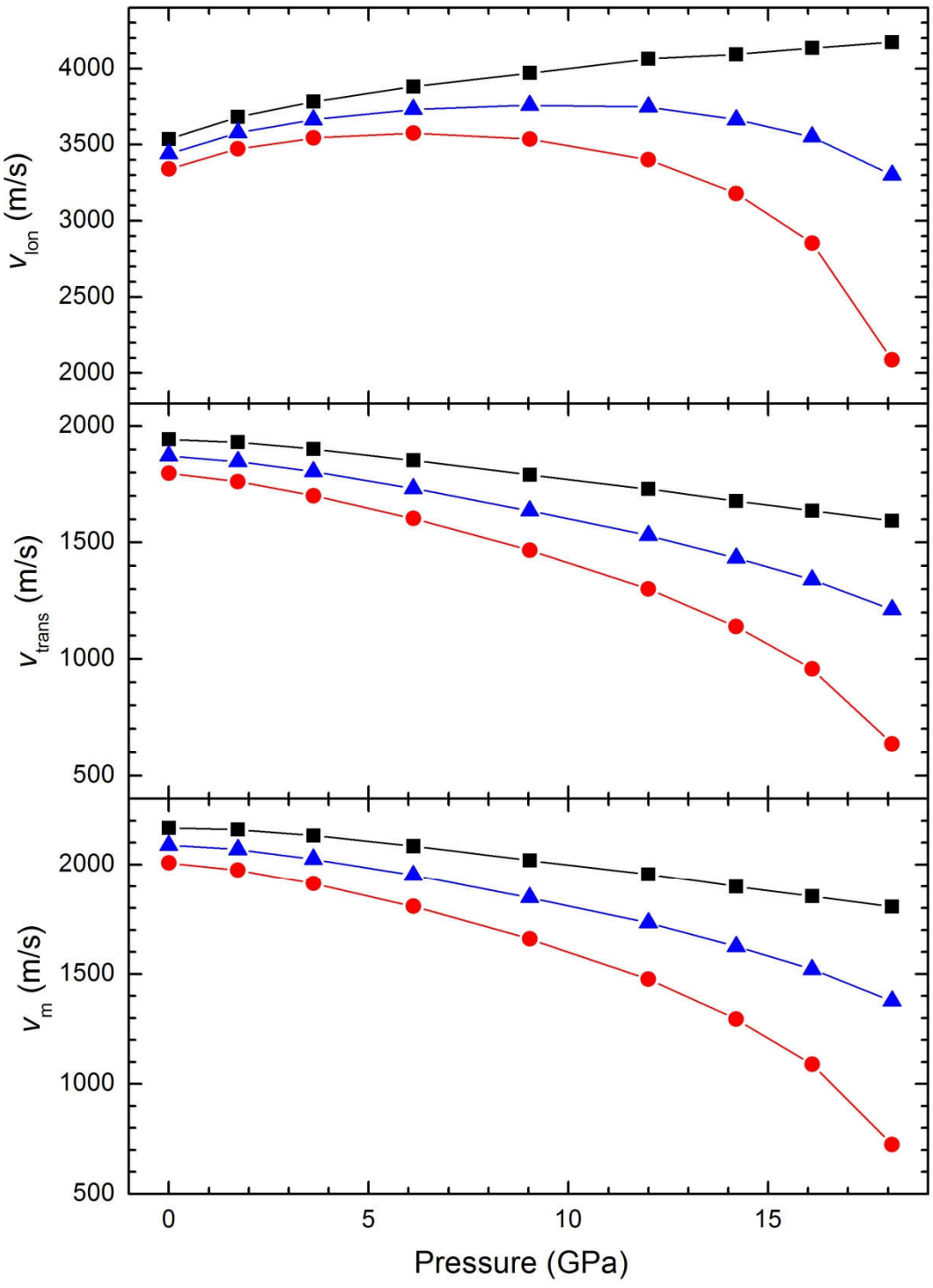

694
695

696 **Figure 9**

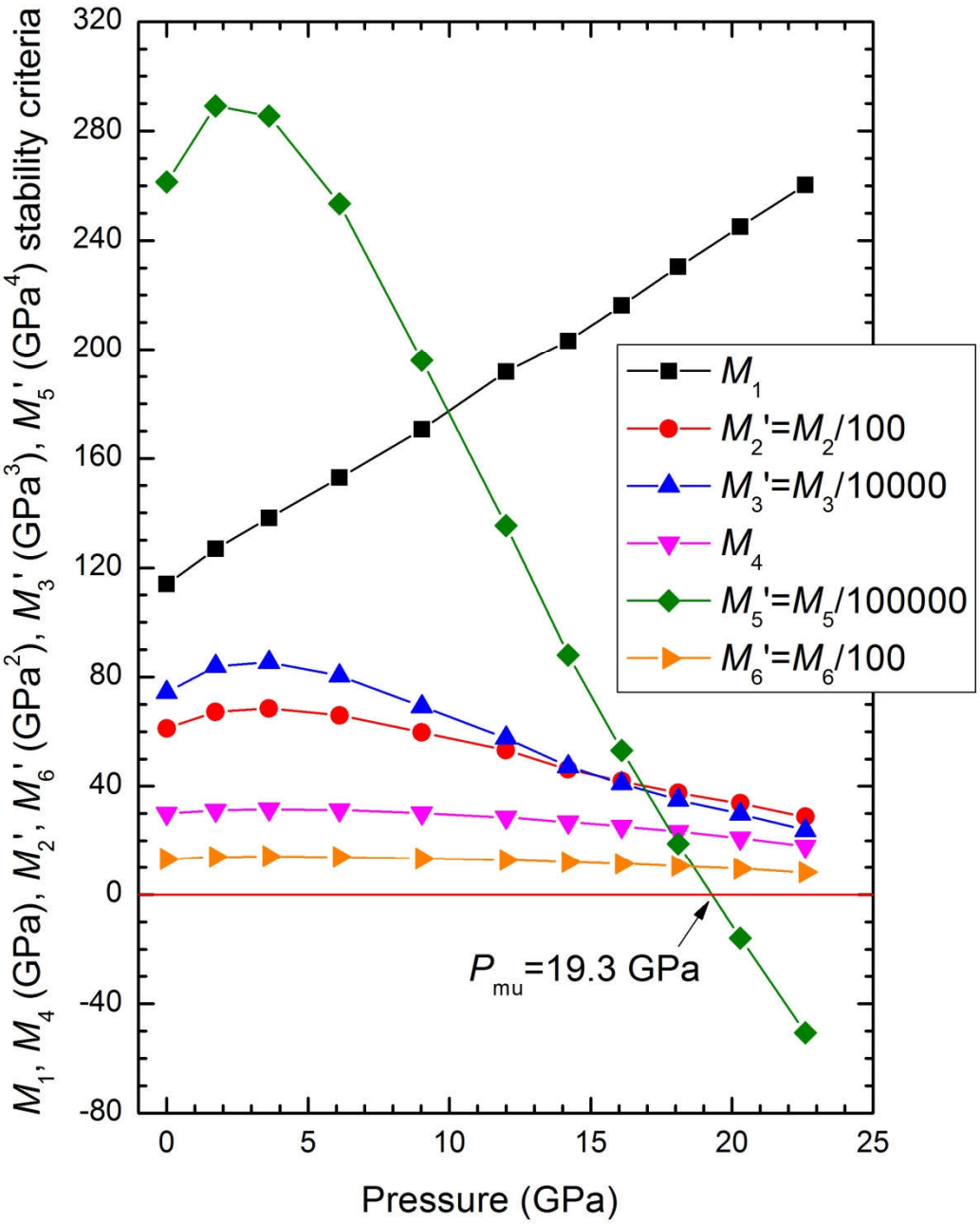

697

698

699 **Figure 10**

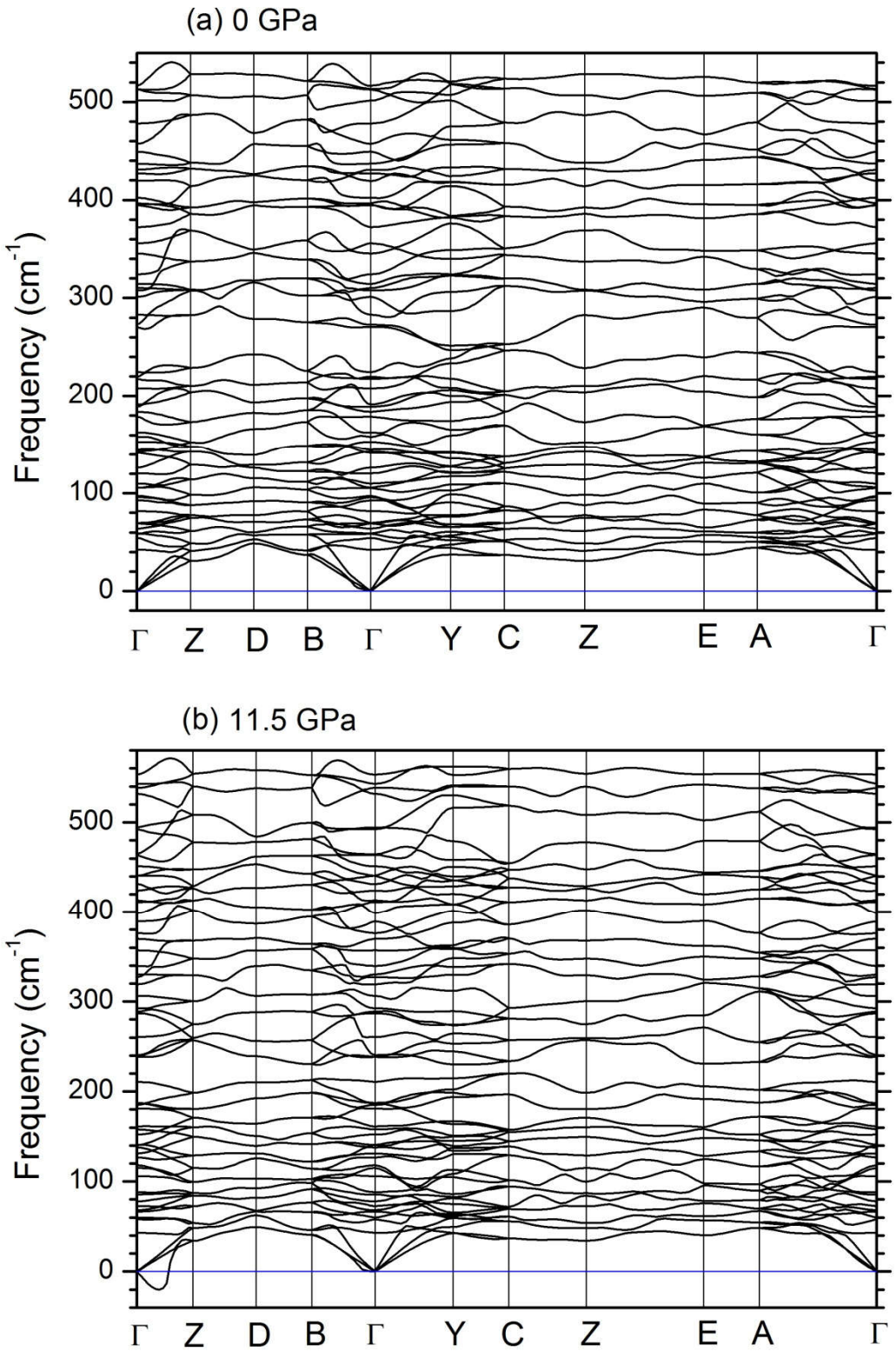

700

701

Figure 11

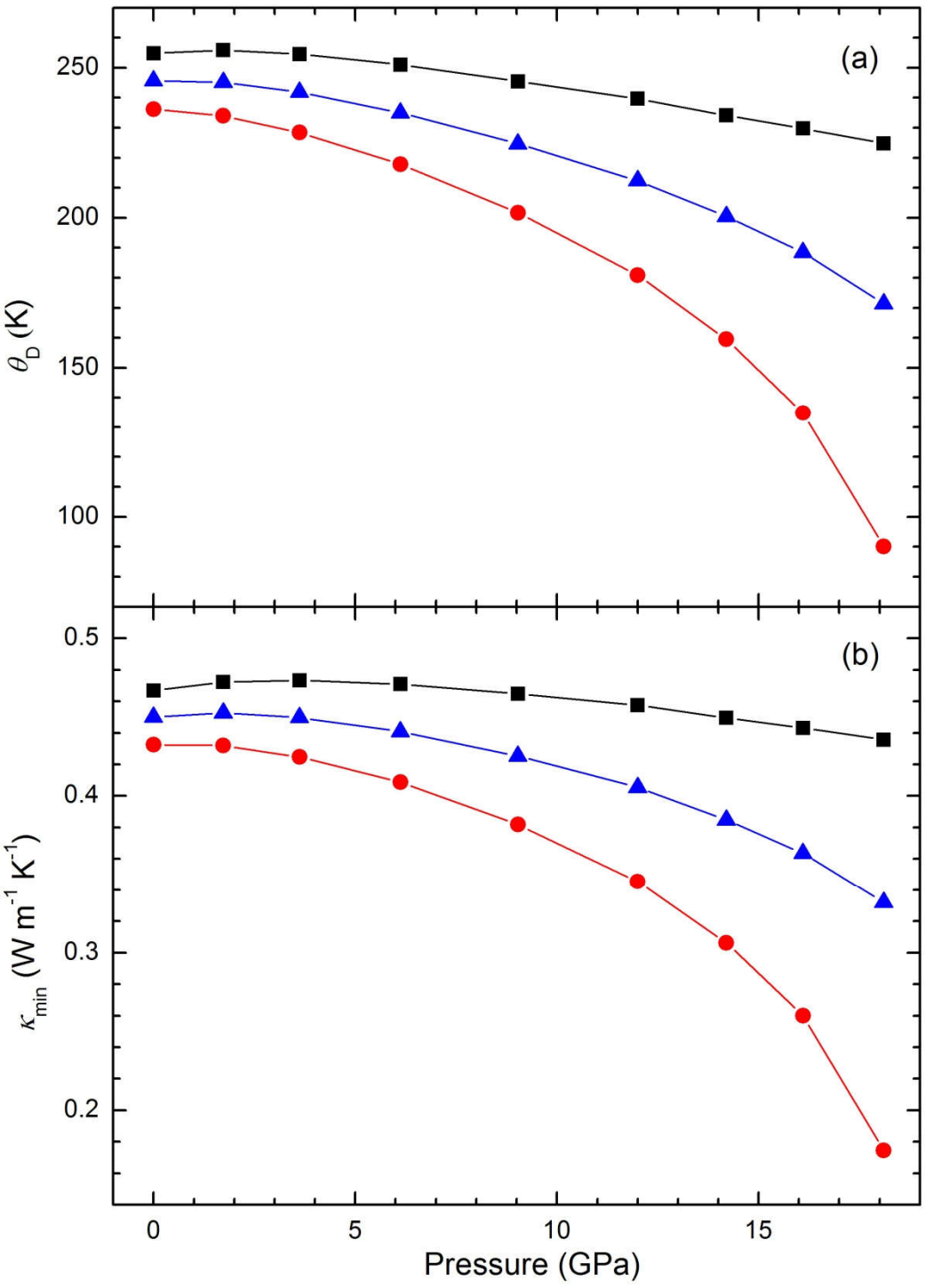
(a)
(b)
θ_D (K)
κ_{min} (W m^{-1} K^{-1})
Pressure (GPa)
250
200
150
100
0.5
0.4
0.3
0.2
0
5
10
15